Journal of Advanced Marine Engineering and Technology, Vol. 50, No. 5, pp. 407~414, 2026
J. Advanced Marine Engineering and Technology (JAMET)
https://doi.org/10.5916/jamet.2026.50.5.407

ISSN 2234-7925 (Print)
ISSN 2765-4796 (Online)
Original Paper

Harvesting magnetic energy from AC power lines for self-powered IoT devices

Kyung-Rak Sohn†

(Received July 8, 2026； Revised July 31, 2026；Accepted October 2, 2026)

Abstract: This paper describes an electromagnetic energy harvesting method that supplies power to an IoT sensor system by capturing stray magnetic fields generated from standard 220 V, 60 Hz household power lines. The goal is to implement a non-contact harvester capable of stably operating under large current fluctuations while efficiently harvesting energy even at low currents. The performance of the proposed energy harvester depends on various key design elements, such as the core material, core volume, number of secondary coil turns, and load resistance. Simulation results indicate that the silicon steel core exhibits a higher magnetic saturation current than conventional ferrite and nanocrystalline alternatives, enabling stable energy harvesting under large current fluctuations in the power lines. Furthermore, the silicon steel core was found to be suitable for the proposed IoT system as it allows for efficient energy harvesting even at low currents. The target IoT prototype is an Arduino-based wireless temperature and humidity sensor node with an operating power of 330mW. By harvesting an average output power of 400mW across a 330 Ω load resistance under a primary current of 5.8 A_{rms}, we successfully and stably operated the sensor node and verified the acquired data on a Bluetooth-connected smartphone.

Keywords: Magnetic field, Energy harvesting, Toroidal magnetic cores, IoT sensor systems

1. Introduction

Internet of Things (IoT)-based wireless sensor systems have been widely deployed to collect data for various localized applications. These systems rely on wireless communication for data transmission, and their operational reliability and scalability depend heavily on the availability of a stable power source. Although conventional replaceable batteries are widely used, they have a limited lifespan and require periodic maintenance and replacement. To overcome these limitations, energy harvesting, which converts ambient energy sources such as light, vibration, pressure, and temperature gradients into electrical energy, has emerged as a promising alternative **[1][2]**.

In **[3]**, an energy harvesting device employing a cantilever piezoelectric bimorph and an NdFeB permanent magnet attached to a space heater power cord carrying 9.4 Arms generated 208 μW at a load resistance of 419 kΩ. However, this output power is insufficient to operate conventional wireless IoT sensor nodes. To address this limitation, coil-based electromagnetic energy harvesters have been proposed **[4]-[6]**. For example, the harvester reported in **[7]** employed a rectangular coil with 1,250 turns wound on an electrical steel core and generated 1.5 W of AC power from a conductor carrying 100 Arms. In **[8]**, a toroidal-core harvester optimized for magnetic saturation produced an induced voltage of 60.9 V from a 60 A current on a 380 V, 60 Hz power line. Another study **[9]** improved the harvested power by connecting five commercial current transformers (CTs) in series. In addition, Sumitomo Electric developed smart grid terminals powered by energy harvested from transmission line currents to monitor conductor temperature and current while wirelessly transmitting the measured data **[10]**. However, these systems weigh approximately 5 kg, exceeding the weight limits specified for vibration monitoring devices (1 kg) and general-purpose monitoring devices (2.5 kg) **[11]**. Therefore, the development of a lightweight energy harvester is essential.

In this study, the performance and feasibility of an energy harvester based on commercially available toroidal-core current transformers (CTs) are investigated. These CTs are compact (50 mm × 20 mm × 25 mm), easy to install, and well suited for low- to medium-current applications. Although they are primarily used for energy monitoring, power quality assessment, and load

† Corresponding Author (ORCID: http://orcid.org/0000-0001-8888-1241): Professor, Division of Electronics Information and Communications Engineering, Korea Maritime & Ocean University, 727, Taejong-ro, Yeongdo-gu, Busan 49112, Korea, E-mail: krsohn@kmou.ac.kr, Tel: +051-410-4312

This is an Open Access article distributed under the terms of the Creative Commons Attribution Non-Commercial License (http://creativecommons.org/licenses/by-nc/3.0), which permits unrestricted non-commercial use, distribution, and reproduction in any medium, provided the original work is properly cited.

Copyright ⓒ The Korean Society of Marine Engineering

analysis, their ring-shaped core, which does not require a primary winding, makes them attractive for magnetic energy harvesting. To efficiently harvest energy from the magnetic field generated by low-current conductors, such as household power lines, the harvester can be optimized by selecting an appropriate number of secondary turns and adjusting the load resistance. Using COMSOL Multiphysics simulations, the optimal design parameters for a lightweight energy harvester capable of reliably powering an Arduino-based IoT sensor system were determined and experimentally validated.

2. System modeling and analysis

As shown in **Figure 1(a)**, the basic structure of a magnetic energy harvester consists of a magnetic core, a primary conductor passing through the center of the core, and a secondary coil. **Figure 1(b)** presents a simplified model for calculating the induced secondary voltage, in which the primary current flows through a single conductor. In this model, a magnetic core with a cross-sectional area (A) is located at a distance (r_i) from the conductor.

The magnetic field B induced around the conductor is expressed by

$$B = \frac{\mu I_{pri}}{2\pi r_i} = \frac{\mu I_0 \sin\omega t}{2\pi r_i} \quad (1)$$

where I_{pri} is assumed to be a pure sinusoidal current with a peak amplitude I_0 and angular frequency ω, and μ denotes the permeability of the core material.

The magnetic flux Φ passing through the core cross-sectional area **[12]** is given by

$$\Phi = \int B \cdot dA = \frac{\mu I_{pri}}{2\pi} \int_{r_i}^{r_o} h \frac{dx}{x} = \frac{\mu I_{pri} h}{2\pi} \ln\left(\frac{r_o}{r_i}\right) \quad (2)$$

In the derivation of the secondary voltage v_{sec} in a coil with N turns, the time-dependent primary current I_{pri} is an independent factor, yielding

$$v_{sec} = \mu h f N I_0 \sqrt{2} \cos\omega t \ln\left(\frac{r_o}{r_i}\right) \quad (3)$$

The root-mean-square (RMS) value of the resulting voltage is then derived as follows.

$$V_{\mathrm{sec\{rms\}}} = \mu h f N I_0 \ln\left(\frac{r_o}{r_i}\right) \quad (4)$$

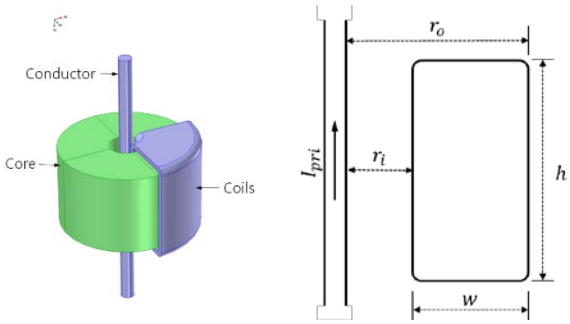

(a) 3D model (b) Cross-section view

Figure 1: Schematic diagram of magnetic energy harvester

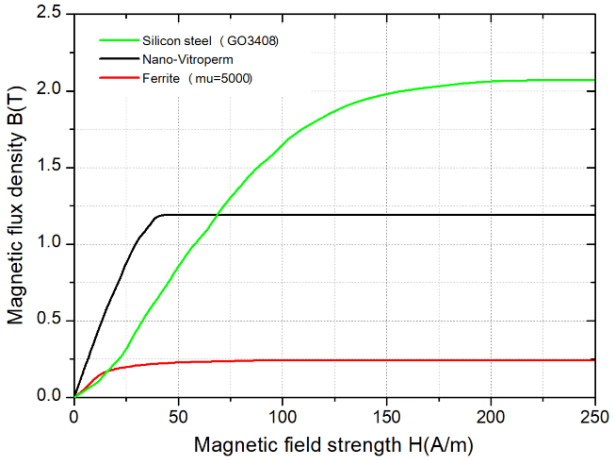

Figure 2: B-H curves of the magnetic cores

To evaluate and compare the energy harvesting suitability of different core materials, the nonlinear B-H curves illustrated in **Figure 2** were incorporated into the FEA (Finite Element Method) model**.** These B-H characteristics were sourced from the verified standard datasets within the COMSOL Multiphysics Material Library, representing typical magnetic properties such as a saturation flux density of 2.1 T for silicon steel GO3408, 1.2 T for nanocrystalline-Vitroperm, and 0.24 T for ferrite J 5000 mu. Based on these simulation parameters, the comparative analysis confirms that silicon steel is the most effective material for high-power harvesting due to its higher saturation threshold.

The simulations were performed in COMSOL Multiphysics using the finite element method (FEM) based on the governing equations implemented in the Magnetic Fields interface of the AC/DC Module. In general, detailed geometric features are not required to construct the simulation model Instead, the dependence on the core's material properties was accounted for by applying the B-H curve of each magnetic material. **Table 1** lists the core dimensions, number of turns, input source, and primary current.

Table 1: Simulation parameters

Parameters	Value
Inner radius (r_i)	10 mm
Outer radius (r_o)	25 mm
Height (h)	25 mm
Number of turns (N)	10-400
Input source (V_s)	220 V, 60 Hz
Peak primary current (I_o)	110 A
Magnetization model	B-H curve

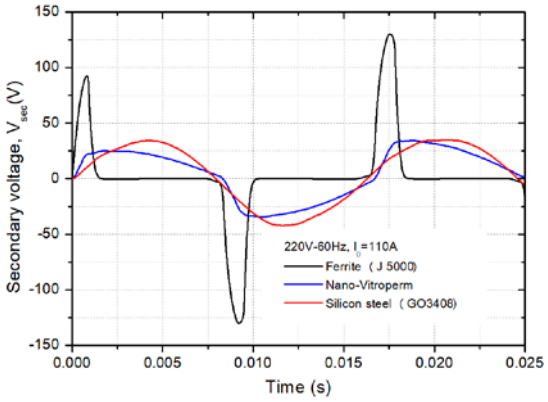

Figure 3: Induced secondary voltage waveform for three different magnetic cores (N=100, I_0=110 A)

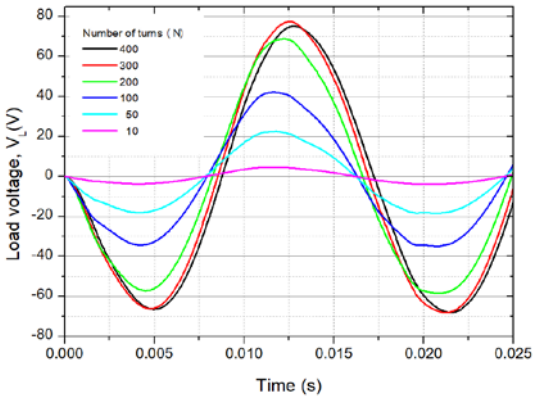

(a) Voltage waveform

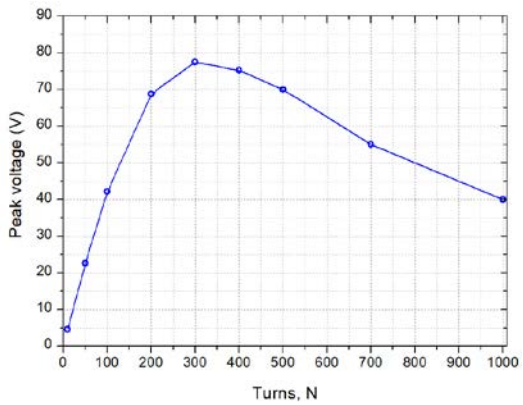

(b) Peak voltage

Figure 4: Output voltage as a function of N (I_0=110 A)

The output voltage waveforms obtained from the COMSOL simulations are shown in **Figure 3**. As illustrated in **Figure 3(a)**, when using a ferrite core, the output signal does not accurately track variations in the input signal. Specifically, the secondary voltage drops sharply to zero when the core enters deep saturation, because the induced voltage is proportional to the time derivative of the magnetic flux. Consequently, an energy harvesting device operating with a saturated magnetic core can deliver power to the load only during the specific intervals of each cycle where the core remains unsaturated. Under identical operating conditions, the nanocrystalline core exhibits only minor waveform distortion, as shown in **Figure 3(b)**. In contrast, the silicon steel core delivers higher output power than the other two materials because the entire periodic waveform is successfully transferred to the load, as demonstrated in **Figure 3(c)**. This performance enhancement is primarily attributed to the superior saturation magnetic flux density of silicon steel.

Figure 4 presents the simulation results illustrating the relationship between the output voltage and the number of turns. For the unsaturated silicon steel core, the output waveform remains undistorted even as the number of turns increases, as shown in **Figure 4(a)**. As the number of turns decreases, the secondary current, which is inversely proportional to the number of turns, increases. However, because the magnetizing inductance (L_m) is proportional to the square of the number of turns, the resulting reduction in output voltage is much greater than the increase in the induced current. Conversely, if the number of turns is increased excessively and approaches infinity, the secondary current becomes negligible, causing the output voltage to approach zero. Considering these two extreme cases, the output voltage reaches a maximum at an intermediate number of turns, as illustrated in **Figure 4(b)**. Therefore, increasing the number of turns does not necessarily result in higher output power. Nevertheless, the simulation results can be used to determine the optimum number of turns required to guarantee the minimum energy harvesting performance needed for the IoT system.

3. Experimental results of energy harvester

Figure 5 shows the fabricated miniature magnetic energy harvester designed for Arduino-based IoT sensor systems. The toroidal core has an inner diameter of 20 mm, an outer diameter of 50 mm, and a height of 25 mm. The primary criterion for selecting the turns was to satisfy the minimum power

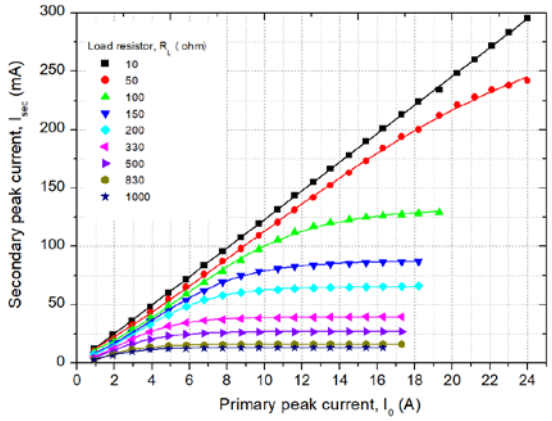

(a) Secondary peak current

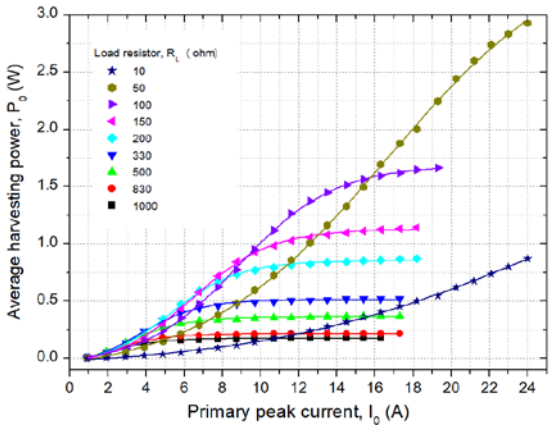

(b) Average harvesting power

Figure 6: Effect of load resistance

requirement of the wireless sensor node while minimizing the winding volume and resistance. In this paper, based on the results in **Figure 4**, a configuration of 70 turns was selected to obtain a 5 V DC output to drive the Arduino, which was achieved by applying a 30 V AC voltage to the rectifier. Furthermore, the experimental results presented in this study demonstrate that the required output power can be customized by appropriately varying the number of turns and the load resistance. The total weight of the fabricated prototype is 330 g. To investigate the effect of load resistance on the energy harvesting performance, a variable resistor was connected across the output terminals of the coil.

Figure 6 illustrates the experimental performance of the fabricated harvester as a function of load resistance. **Figure 6(a)** plots the induced secondary current against the primary current for different load resistances. When the load resistance is as low as 10 Ω, the induced current is approximately proportional to the primary current. However, as the load resistance increases, magnetic core saturation occurs at lower primary current levels. Once the core becomes deeply saturated, the magnetic flux no longer varies significantly, causing the secondary current to reach a plateau and remain nearly constant. Since typical IoT sensor systems consume very little power and therefore draw only a small load current, the harvester can be approximated as a secondary coil operating under no-load conditions. **Figure 6(b)** presents the average harvested power, calculated from the induced current, as a function of the primary current for different load resistances. For load resistances of 100 Ω or greater, the harvested power reaches saturation when the primary current exceeds approximately 10 A. Based on these experimental results, the optimum load resistance can be determined by considering both the available primary current and the power requirements of the target IoT system.

When the open window of the output waveform reaches its maximum, the maximum harvest power (P_{max}) is calculated using the matched impedance condition **[13]**.

$$P_{(max)} = \frac{1}{2}\left(\frac{I_0}{N}\right)^2 R_{L(sat)} \tag{5}$$

The saturation load resistance $R_{L(sat)}$ that forces the magnetic core into saturation can be derived directly from the relationship between the secondary induced voltage and the primary peak current I_0. Since the secondary voltage is developed across the load R_L and the internal secondary coil winding resistance R_s, setting $V_{sec} = V_{sec(max)}$ allows us to isolate the saturation-limiting load resistance as a function of the primary current. To clearly illustrate how the variable load resistance R_L contributes to the core saturation, the final expression was adopted directly from Reference **[13]** without further detailed derivation, and is simplified as follows:

$$R_{L(sat)} \simeq \frac{\omega N^2 B_{sat} A}{I_0} \tag{6}$$

where B_{sat} is the saturation flux density of the magnetic core.

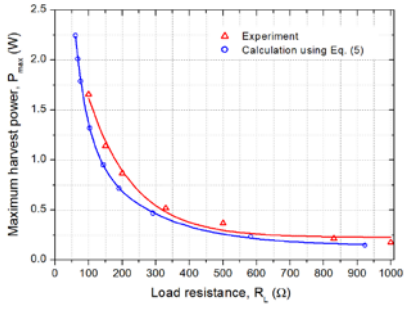

Figure 7: Maximum power harvest with respect to the load resistance

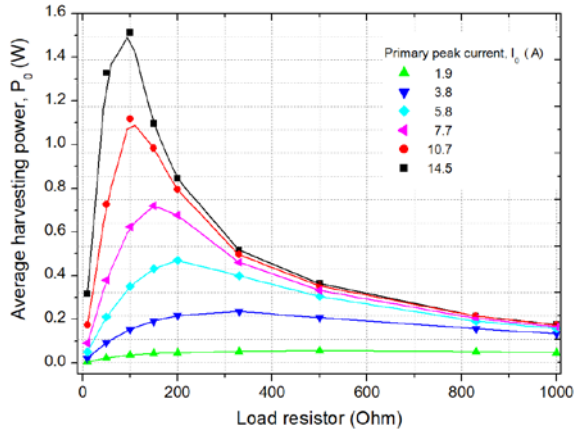

Figure 8: Average harvesting power delivered to the resistive load

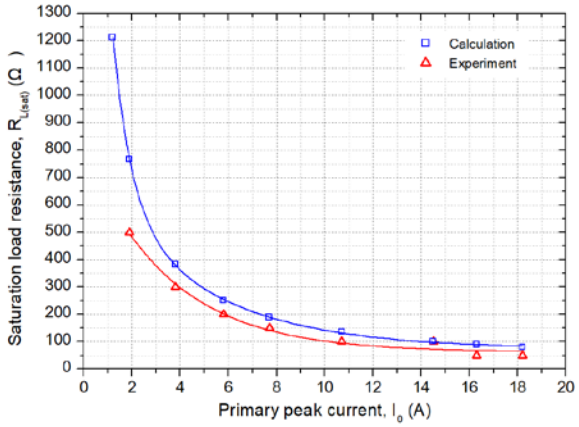

Figure 9: Saturation load resistance with respect to the primary current (B_{sat}=2.1 T)

Based on the structural and material parameters of the fabricated harvester, the maximum harvested power as a function of load resistance can be calculated via **(5)**. The corresponding experimental data were obtained from **Figure 6(b)**. As shown in **Figure 7**, the analytical predictions agree well with the experimental results, demonstrating excellent consistency between the two. When the load resistance exceeds the threshold saturation resistance, the magnetic core enters a deeper state of saturation, and the harvested power no longer increases.

Figure 8 illustrates the average harvested power as a function of load resistance for different primary currents. When the load resistance is below 100 Ω, the magnetic core remains unsaturated, and the harvested power increases with increasing load resistance. In contrast, as the load resistance approaches infinity, the induced secondary current approaches zero, resulting in negligible power transfer. Consequently, an optimal load resistance exists between these two extremes, at which the harvested power reaches its maximum value. For example, at a primary current of 5.8 A_{rms}, a maximum average harvested power of 500 mW is achieved with the optimal load resistance of 200 Ω. Although operating at this optimal 200 Ω condition ensures a higher power margin, a 330 Ω load resistance, which yields a slightly lower average power of 400 mW, was intentionally selected for the practical sensor integration experiment. This choice was made to robustly demonstrate that the proposed harvester can reliably drive the target Arduino-based IoT wireless sensor system, even under a non-optimal load condition that closely mimics the actual application environment.

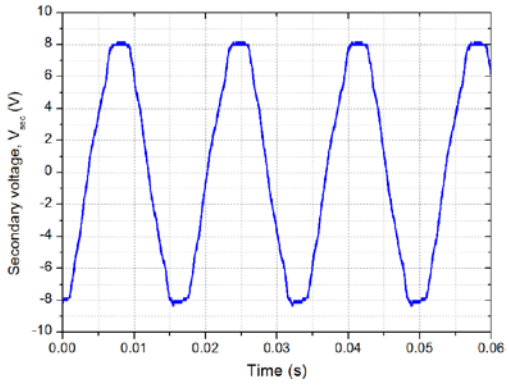

(a) $R_L = 100\ \Omega$ (No saturation)

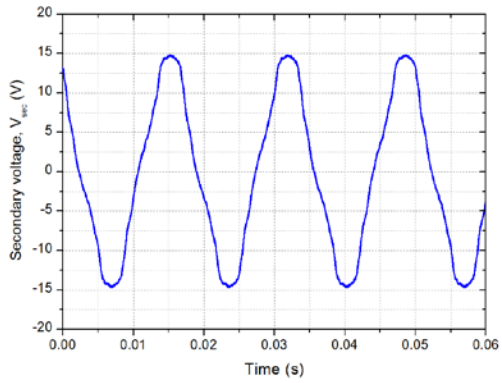

(b) $R_L = 200\ \Omega$ (Soft saturation)

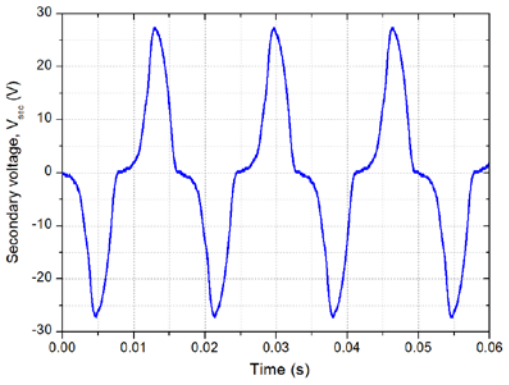

(c) $R_L = 500\ \Omega$ (Strong saturation)

Figure 10: Output voltage waveform (I_{pri} = 5.8 A, N = 70)

The minimum load resistance required to induce magnetic core saturation is calculated using **(6)**, while the corresponding experimental values are obtained from the data presented in **Figure 8**. As shown in **Figure 9**, the analytical predictions agree well with the experimental results. Furthermore, the critical load resistance required to induce core saturation decreases as the primary current increases.

Figure 10 presents the measured output voltage waveforms at a primary current of 5.8 A_{rms} under different load conditions. At a load resistance of 100 Ω, the magnetic core remains unsaturated, resulting in an undistorted output waveform with a peak voltage of 8 V, as shown in **Figure 10(a)**. When the load resistance is increased to 200 Ω, the peak voltage rises to 15 V, and slight waveform distortion becomes evident, as illustrated in **Figure 10(b)**. Under this condition, the core operates in a soft saturation region, corresponding to the maximum power harvesting condition. When the load resistance is further increased to 500 Ω, the core enters deep saturation. As shown in **Figure 10(c)**, the unsaturated interval is reduced to less than half of the AC cycle, indicating that the induced voltage is generated only during a limited portion of the cycle. These results demonstrate that increasing the load resistance causes the magnetic core to saturate at lower primary currents, thereby reducing the conduction interval of the output voltage waveform.

4. Self-powered IoT device test

As shown in **Figure 11(a)**, the proposed self-powered sensor system consists of three main components: an energy harvester, a rectifier circuit, and a wireless sensor node. The AC voltage induced in the harvesting coil is converted into a regulated DC voltage using a full-wave bridge rectifier followed by a linear voltage regulator. **Figure 11(b)** shows the fabricated IoT sensor system integrated with the custom-designed energy-harvesting power supply. The rectification stage employs an 8 A single-phase bridge rectifier and an LM1117 linear voltage regulator. The wireless sensor node comprises an Arduino Uno microcontroller interfaced with a DHT-11 temperature and humidity sensor and an HC-06 Bluetooth module.

The peak power consumption of the proposed system, measured using a power meter (HPM-100A, AD POWER), is 330mW. To satisfy this power requirement, a primary current of 5.8 A_{rms} and a load resistance of 330 Ω were selected. The standalone IoT sensor node draws an extremely low current during its operation, allowing its intrinsic input impedance to be approximated as a no-load condition relative to the harvester.

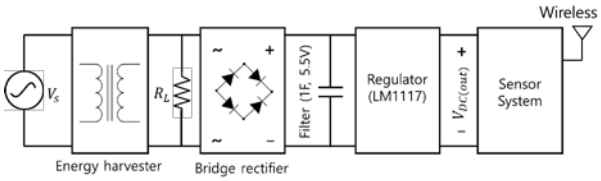

(a) Block diagram



(b) Experimental setup and smartphone monitoring application

Figure 11: Arduino-based self-powered IoT sensor system

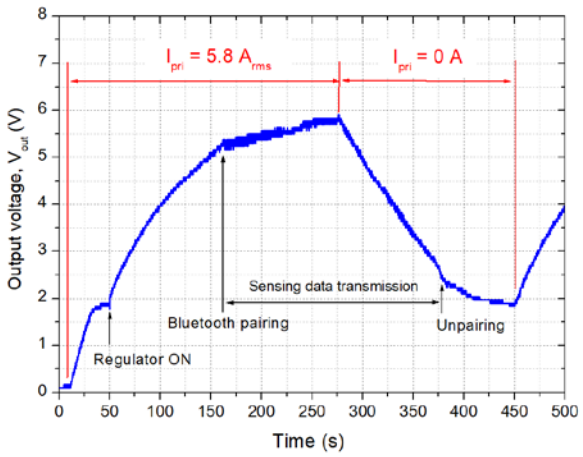

Figure 12: Response of the energy harvester according to the operating conditions of the wireless node

However, to induce magnetic core saturation and enable effective power extraction, a dedicated load resistance is required. As illustrated in the system schematic in **Figure 11(a)**, a 330 Ω load resistor is physically implemented between the energy harvester and the rectifier. According to the experimental results shown in **Figure 8**, the harvesting system can supply 400mW of power by successfully driving the core into saturation with a 330 Ω load. This meets the 330mW power consumption requirement of the fabricated IoT sensor system. The primary current was monitored using a clamp meter throughout the experiment. Once the Arduino Uno establishes a Bluetooth connection with a smartphone via the HC-06 module, the measured temperature

and humidity data are transmitted at 1 s intervals. The transmitted data were successfully received and verified using a custom-developed smartphone application, as shown in **Figure 11(b)**.

Figure 12 illustrates the transient response of the harvested voltage under different operating conditions of the wireless sensor system at a primary current of 5.8 A_{rms}. When the voltage across the smoothing filter capacitor reaches 2 V, the voltage regulator is activated, resulting in additional power consumption. As the capacitor voltage approaches 5 V, the Bluetooth module initiates the pairing process, and wireless data transmission begins. Conversely, when the primary current is cut off and the capacitor voltage drops below 2.5 V, the Bluetooth connection is terminated. When the primary current is applied again, the energy harvesting system recharges the smoothing capacitor, and the sensor node resumes operation.

5. Conclusion

In this study, a compact magnetic energy harvester for self-powered wireless sensor applications was proposed and experimentally validated. The operational characteristics of the harvester were comprehensively analyzed through both COMSOL Multiphysics simulations and experimental verification. Among the evaluated magnetic core materials, silicon steel exhibited a higher saturation magnetic flux density than ferrite and nanocrystalline alloys, confirming it as the most suitable material for high-power-density magnetic energy harvesting. In addition, the relationship between the number of turns and the harvested power was investigated. The results indicate that increasing the number of turns does not necessarily yield a proportional increase in harvested power. Therefore, a careful optimization of the coil turns is required to meet the power demands of the target sensor system. Furthermore, maximum power extraction is achieved only when the load resistance exceeds the threshold required to induce magnetic core saturation.

The energy harvester fabricated in this study achieved a power density of 9.7 mW/cm³, utilizing a compact silicon steel core with a volume of 41.2 cm³, configured with 70 coil turns and a 330 Ω load resistance. Moreover, the device successfully powered an Arduino-based IoT wireless sensor system without any external power supply, demonstrating its viability as a self-sustained power source for various industrial IoT applications.

Acknowledgement

This research was supported by the ANCHOR program through Busan Anchor Center, funded by the Ministry of Education (MOE) and the Busan Metropolitan City, Republic of Korea.

Author Contributions

Conceptualization, K.R.Sohn; Methodology, K.R.Sohn; Software, K.R.Sohn; Formal Analysis, K.R.Sohn; Investigation, K.R.Sohn; Resources, K.R.Sohn; Data Curation K.R.Sohn; Writing-Original Draft Preparation, K.R.Sohn; Writing-Review & Editing, K.R.Sohn; Visualization, K.R.Sohn; Supervision, K.R.Sohn; Project Administration, K.R.Sohn; Funding Acquisition, K.R.Sohn.

References

[1] X. Tang, X. Wang, R. Cattley, F. Gu, and A. D. Ball, “Energy harvesting technologies for achieving self-powered wireless sensor networks in machine condition monitoring: A review,” Sensors, vol. 18, no. 4113, pp. 1-39, 2018. https://doi.org/10.3390/s18124113.

[2] M. Grossi, “Energy harvesting strategies for wireless sensor networks and mobile devices: A review,” Electronics, vol. 10, no. 661, pp. 1-53, 2021. https://doi.org/10.3390/electronics 10060661.

[3] E. S. Leland, R. M. White, and P. K. Wright, “Energy scavenging power sources for household electrical monitoring,” in proc. of The Sixth International Workshop on Micro and Nanotechnology for Power Generation and Energy Conversion Applications, pp. 165-168, 2006.

[4] H. Zangl, T. Bretterklieber and G. Brasseur, “Energy harvesting for online condition monitoring of high voltage overhead power lines,” in proc. of IEEE International Instrumentation and Measurement Technology Conference, Canada, May, 2008. https://doi.org/ 10.1109/IMTC.2008.4547255.

[5] V. Gupta, A. Kandhalu, and R. Rajkumr, “Energy harvesting from electromagnetic energy radiating from AC power lines,” in proc. of the 6th Workshop on Hot Topics in Embedded Networked Sensors, No. 17, pp. 1–6, June 2010, https://doi.org/10.1145/1978642.1978664.

[6] F. Guo, H. Hayat, and J. Wang, “Energy harvesting devices for high voltage transmission line monitoring,” in proc. of IEEE Power and Energy Society General Meeting, pp. 1-8, 2011. https://doi.org/10.1109/PES.2011.6039037.

[7] R. M. White, D. -S. Nguyen, Z. Wu, and P. K. Wright, “Atmospheric sensors and energy harvesters on overhead power lines,” Sensors, vol. 18, no. 114, pp. 1-7, 2018. https://doi.org/10.3390/ s18010114.

[8] B. Park, D. Kim, J. Park, K. Kim, J. Koo, H. Park, and S. Ahn, “Optimization design of toroidal core for magnetic energy harvesting near power line by considering saturation effect,” AIP Advances, vol. 8, 056728, pp. 1-6, 2018. https://doi.org/10.1063/1.5007772.

[9] K. R. Sohn and H. S. Kim, “A magnetic energy harvesting device using current transformer,” J. Advanced Marine Engineering and Technology, vol. 45, no. 5, pp. 307-311, 2021. https://doi.org/10.5916/jamet.2021.45.5.307

[10] M. Sanda, T. Kojima, E. Higahi, T. Maruyama, N. Iwama, and O. Sakai, “Overhead Transmission Line Monitoring System for Dynamic Rating,” SEI Technical Review, no. 87, pp. 64-69, 2018.

[11] Y. Liu, X. Xie, Y. Hu, Y. Qian, G. Sheng, X. Jiang, and Y. Liu, “A novel high-density power energy harvesting methodology for transmission line online monitoring devices,” Rev. Sci. Instrum. vol. 87, 075119, pp. 1-8, 2016. https://doi.org/10.1063/1.4959556.

[12] O. Thorin, “Power line induction energy harvesting powering small sensor nodes,” M. S. Thesis, Dept. Machine Design, KTH, Stockholm, Sweden, 2016.

[13] J. Moon and S. B. Leeb, “Analysis Model for Magnetic Energy Harvesters,” IEEE Trans. Power Electron. vol. 30, no. 8, pp. 4302-4311, 2015. https://doi.org/10.1109/TPEL.2014.2357448.